J Appl Electrochem (2013) 43:147–158
DOI 10.1007/s10800-012-0496-z

ORIGINAL PAPER

Ethanol oxidation on a high temperature PBI-based DEFC using Pt/C, PtRu/C and Pt_3Sn/C as catalysts

José J. Linares · Sabrina C. Zignani · Thairo A. Rocha · Ernesto R. Gonzalez

Received: 30 July 2012 / Accepted: 22 October 2012 / Published online: 7 November 2012
© Springer Science+Business Media Dordrecht 2012

Abstract A high temperature ethanol-fed polymer electrolyte membrane fuel cell has been implemented by using H_3PO_4-doped *m*-polybenzimidazole as polymeric electrolyte. Commercial Pt/C, PtRu/C and Pt_3Sn/C catalysts are used in the anode. The performance was assessed in terms of polarization curves at different temperatures, feeding the cell with a high concentration ethanol solution (water/ethanol mass ratio of 2). The product distribution was measured with the support of a gas chromatograph. The use of bimetallic catalysts increased the current density. PtRu/C showed the best performance up to 175 °C, but it is outperformed by Pt_3Sn/C at 200 °C. In terms of oxidation products, higher temperatures and current densities favour the oxidation of ethanol. However, Pt_3Sn/C promoted the generation of more oxidized products compared to PtRu/C (in which most of the ethanol is oxidized to acetaldehyde), especially at high temperature. This accounts for the large current density. In terms of complete oxidation of ethanol to CO_2, Pt/C was by far the most efficient catalyst for C–C scission, achieving percentages of 56 % of CO_2, although operating above 175 °C dramatically boosted an undesirable methanation process that slashed the efficiency. The combination of fuel cell results and product distribution helped to suggest the different oxidation routes on the surface of the different catalysts.

J. J. Linares · S. C. Zignani · T. A. Rocha · E. R. Gonzalez (✉)
Instituto de Química de SãoCarlos, USP, Av. Trabalhador São Carlense, 400, CP 780, São Carlos, SPCEP 13560-970, Brazil
e-mail: ernesto@iqsc.usp.br

Present Address:
J. J. Linares
Instituto de Química, Universidade de Brasília, Campus Darcy Ribeiro CP 04478, Brasília, DF CEP 70910-000, Brazil

Keywords PEMFC · Ethanol · Oxidation products · High temperature · Polybenzimidazole · Catalysts

1 Introduction

One of the most stringent limitations for the development of direct ethanol fuel cells (DEFC) operated with a polymer electrolyte membrane (PEM) is the low efficiency for the total conversion of ethanol to carbon dioxide [1]. Although for low scale portable applications such an issue is not so crucial, for larger scale ones, e.g., automotive, it is necessary to overcome this limitation [2]. In this sense, one of the alternatives is the operation at higher temperature than traditional Nafion®-based DEFC (limited to 90 °C), so that the system possesses more energy for breaking the C–C bond [3]. The use of phosphoric acid impregnated *m*-polybenzimidazole (m-PBI) allows the increase of the operational temperature up to 200 °C [4–7] with good proton conductivity. Another remarkable advantage of this material is the low ethanol crossover [8], opening the possibility of operation with high ethanol concentrations, very interesting from a practical point of view.

Catalyst development is another way in order to improve the performance of ethanol-fed PEMFC. Platinum, which is the most active catalyst in acidic environment, is known to be severely poisoned by adsorbates generated during the ethanol oxidation. These can be only removed at high potentials, where Pt–OH species are generated on the surface of the electrode. In order to overcome this, it has been proposed the combination of platinum with a second, less noble metal, for example, ruthenium, tin, tungsten, rhodium, osmium, nickel, molybdenum [9–15]. Nevertheless, among the spectrum of bimetallic catalysts, PtRu/C and Pt_3Sn/C have emerged as the most suitable ones [16–19].

They are known to promote the ethanol oxidation process by two mechanisms [9, 18, 20]: (i) bifunctionality: the second metal provides the oxidized species (–OH) required for the renewal of the platinum surface at lower potentials compared to platinum, and (ii) electronic effect: modification of the adsorption energies of the ethanolic residues. In most cases, both effects are present.

However, so far, few studies have been devoted to this type of high temperature ethanol-fed PEMFC systems. Sun et al. [21] reported the beneficial effect of high temperatures for increasing the conversion of ethanol to CO_2, although using quite low ethanol concentrations (0.01 and 0.1 M), achieving CO_2 percentages as high as 90 % at 100 °C from the results of a differential electrochemical mass spectrometry study. In vapour-fed systems, Wang et al. [3] reported an early study of the performance of a high temperature PBI-based DEFC, operating at 170 °C, opening the possibility of mounting such a system, with a high ethanol conversion to CO_2 (up to 35 %), using Pt and PtRu black as catalysts. Later, Lobato et al. [8] designed a high temperature vapour-fed DEFC with the same electrolyte, showing satisfactory values of the power density compared to other high temperature DEFC systems. Afterwards, the same research group developed catalysts of different nature for application in this system [22, 23]. Parrondo et al. [24] also showed some interesting results on the application of In_2O_3 combined with Pt as catalyst. Uda et al. [25], Otomo et al. [26, 27] and Shimada et al. [28] have recently operated a vapour-fed DEFC with CsH_2PO_4 as electrolyte at temperatures between 200 and 300 °C, obtaining interesting results in terms of high ethanol conversion to carbon dioxide, corroborating the previous results obtained by Wang et al. Indeed, Otomo et al. [28] showed a higher level of conversion of ethanol to carbon dioxide, achieving a percentage of C_1 products of almost 90 %. Nonetheless, in its complete analysis, they highlighted the appearance of methane as by-product at high temperature. Finally, in a recent paper, this research group [11] has demonstrated the advantages of operating an ethanol-fed PEMFC system at high temperatures (150 and 200 °C) in terms of an enhanced CO_2 percentage produced.

With these considerations, the operation at temperatures above 100 °C can be considered as an alternative for overcoming the limitations of the DEFC. In this sense, this paper proposes the use of the most typical bimetallic catalysts (commercial PtRu/C and Pt_3Sn/C), compared with commercial Pt/C, evaluating the cell performance in terms of polarization and power density curves, and measuring the product distribution with an online gas chromatograph coupled to the anode exhaust. The analysis was performed at different temperatures and current densities, allowing the proposal of possible mechanisms for the ethanol oxidation on the different catalysts and under the studied operation conditions. This might help to further understand the performance of the catalysts, and propose new formulations with the goal of maximizing performance and efficiency of conversion of ethanol to CO_2.

2 Experimental

Commercial 20 % Pt/C, 20 % PtRu/C and 20 % Pt_3Sn/C from BASF Fuel Cell (former ETEK-Inc.) were the catalysts used for this study. For the different catalyst powders, X-ray diffraction (XRD) patterns were recorded on a Rigaku Ultima IV (Rigaku Corp., Japan) from 20° to 90° (0.02° step, 2° min^{-1}) in order to assess the crystalline structure of the different materials. The corresponding gas diffusion electrodes were prepared as follows. A diffusion layer was made of carbon powder (Vulcan XC-72R) and 15 wt% Teflon TE-3893 (Dupont), and the mixture was applied homogeneously over a carbon cloth (PWB-3, Stackpole) by vacuum filtration. Onto this layer, for the anode, a catalyst layer was brush-applied until attaining a platinum loading of 2 mg cm^{-2}, with 10 wt% Teflon as binder. In the case of the cathode, the Pt loading was 1 mg cm^{-2}, using the same percentage of Teflon. Two electrodes with an active geometric area of 4.62 cm^2 were sandwiched on both sides of a commercial PBI membrane (Daposy, Denmark) previously immersed in 85 % H_3PO_4. The use of this highly concentrated bath makes unnecessary the impregnation of the electrodes with phosphoric acid. Hot pressing was carried out at 1 tonne and 150 °C for 15 min. MEAs prepared were stored in sealed plastic bags until future use in the fuel cell.

The experimental setup for the fuel cell experiments consisted of a peristaltic pump to impel the liquid fuel mixture to a stainless steel vaporizer heated at 170 °C in order to guarantee the complete evaporation of the fuel. The polarization curves were recorded under linear sweep voltammetry conditions, cycling at a scan rate of 0.2 mV s^{-1}, trying to simulate pseudo-stationary conditions. They were recorded with the aid of a potentiostat/galvanostat AUTOLAB PGSTAT 302 (Ecochemie) equipped with a current booster of 20 A. The operating temperatures were 130, 150, 175 and 200 °C, using an ethanol:water weight ratio of 1:2 [8], corresponding approximately to a molar concentration of 6.7 mol L^{-1}, at a flow rate of $\approx$0.17 mL min^{-1}. The oxygen flow was 0.1 L min^{-1} at atmospheric pressure.

The fuel cell hardware consisted of two graphite monopolar plates, into which a four-channel serpentine geometry was machined. Within the graphite plates, heating rods were fitted in order to heat up the cell. The temperature was controlled with the aid of a temperature controller (Flyever). Onto this graphite plate, the voltage

probes were drilled. The endplates were made of aluminium, with a compressible graphite foil in order to minimize the contact resistance. The current collectors were placed on both endplates.

For the determination of the product distribution, a gas chromatograph was coupled online to the anode exhaust. The cell was operated under galvanostatic conditions for at least 2 h, awaiting a stable value of the current density. The connecting pipe consisted of a stainless steel 1/16″ outer diameter pipe, onto which a flexible silicone heating mantle was wrapped. The temperature of the pipe was kept at 150 °C in order to avoid the condensation of the oxidation products, specially acetic acid and ethyl acetate. The temperature was controlled with the aid of a temperature controller. This pipe carried the vapour into a regulating loop responsible for the injections in the gas chromatograph. For the separation, a PORAPAK-Q column was used, using helium as mobile phase. A temperature ramp from 60 to 180 °C (10 °C min^{-1}) was programmed, allowing the desired separation of all the compounds. The required analysis time was 35 min. TCD (mainly for CO_2) and FID (all combustible products: acetaldehyde, acetic acid, methane, ethyl acetate) detectors were simultaneously used in order to guarantee the complete identification of all the products. Their quantification was possible because of the previous calibration made with the different possible products obtained from the ethanol oxidation according to the literature [3, 28–33]. Images of the experimental setup are shown in Fig. 1.

3 Results

Table 1 collects the most significant information obtained from the diffractograms of the different catalysts. As it can be seen, the crystal size for all the catalysts is in the nanometric range, from 2 to 4 nm, with a larger value for the Pt_3Sn/C catalyst. Nevertheless, the most relevant information comes from the lattice constant of the different catalysts. As it can be seen in Table 1, the presence of ruthenium leads to a drop of that parameter compared to that of the Pt fcc crystalline structure. This implies the formation of a PtRu solid solution whose composition can be calculated by Vegard's law [11]. In the case of tin, there is an increase in the lattice parameters of platinum, indicative of the formation of a crystalline Pt_3Sn phase ($a_{Pt_3Sn} = 0.4001$ nm). Other crystalline phases that can be formed are most likely absent, since no other peaks appeared in the diffractograms. Again, by the application of Vegard's law [34], it is possible to estimate the degree of alloy.

Table 1 Main structural parameters obtained from DRX for the different catalysts

Catalyst	Crystal size/nm	Lattice parameter/nm	Secondary metal fraction in the alloy	% of secondary metal in the alloy
Pt/C	2.3	3.923	–	–
PtRu/C	2.9	3.895	0.22	28.2
Pt_3Sn/C	3.9	3.996	0.23	93.6

The results summarized in Table 1 confirm the formation of a $Pt_{0.88}Ru_{0.22}$ fcc solid solution, corresponding to a 28.2 % of the ruthenium inserted in the Pt fcc structure. The rest is expected to be in the form of amorphous ruthenium oxide or a segregated metallic amorphous phase. In the case of tin, 93.6 % of the tin is forming the Pt_3Sn fcc crystalline phase, virtually showing a complete Pt_3Sn alloy, whereas the rest is most likely in the form of SnO_2 [35].

Polarization and power density curves of the different catalysts at 130, 150, 175 and 200 °C are shown in Fig. 2. First, the use of a bimetallic catalyst is significantly beneficial in terms of polarization (current density) and power density performance. However, there is a significant

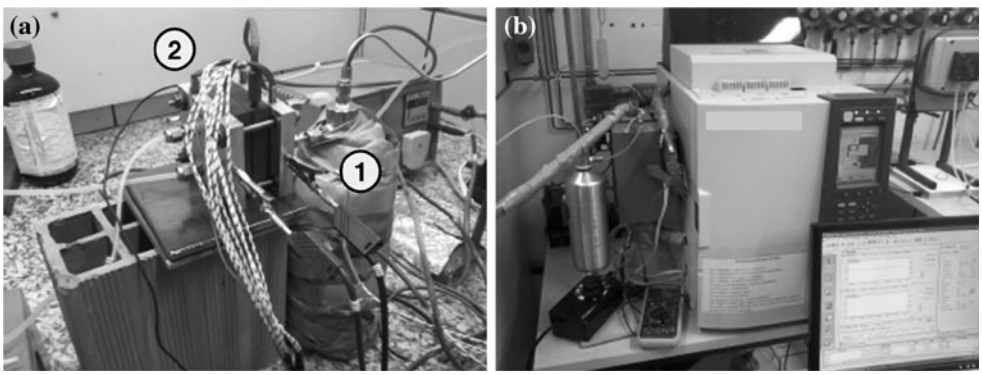

Fig. 1 **a** Images of the fuel cell system used for the electrochemical measurements (*1* vaporizer, *2* fuel cell rig), **b** gas chromatograph coupled to the fuel cell

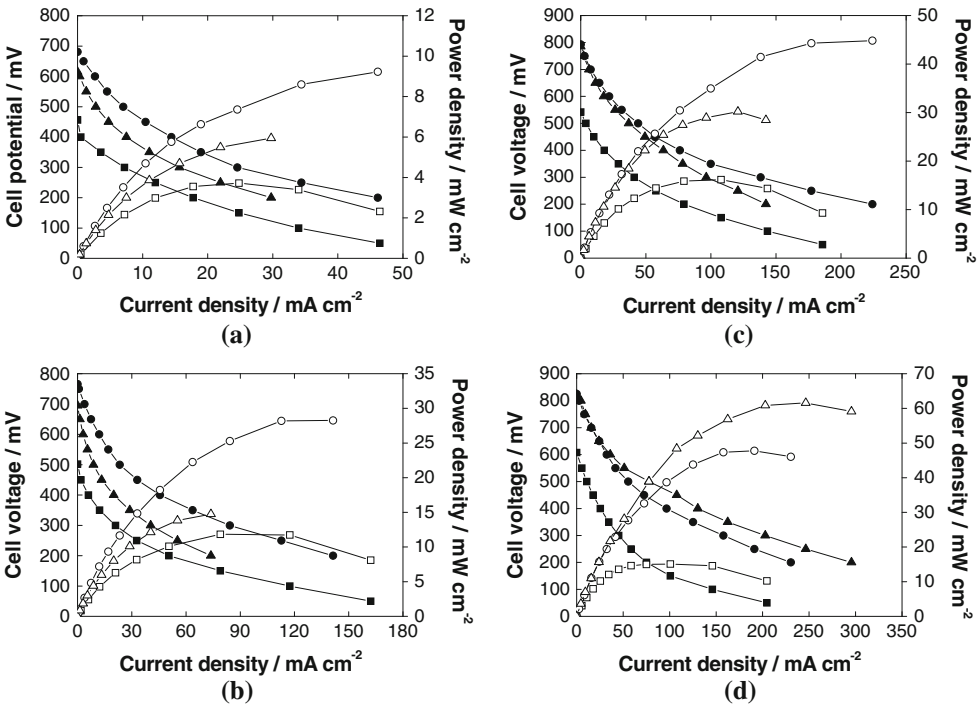

Fig. 2 Fuel cell polarization and power density curves at **a** 130 °C, **b** 150 °C, **c** 175 °C and **d** 200 °C (*filled and open square* Pt/C, *filled and open circle* PtRu/C, *filled and open triangle* Pt_3Sn/C; *solid symbols* polarization curves, *hollow symbols* power density curves)

change in the behaviour of the bimetallic catalysts with the temperature. At the lowest temperature, PtRu/C displays the best performances, whereas at 200 °C, the most efficient catalyst in terms of current density is Pt_3Sn/C. This also reflects on the maximum power density shown in Fig. 3. The maximum power density for ethanol oxidation at 175 °C was for the PtRu/C catalyst, with a value of 44.8 mW cm^{-2}, whereas at 200 °C, the maximum power density was that of Pt_3Sn/C, with a value of 61.6 mW cm^{-2}. Looking more in detail, there is a significant decrease in the enhancement of the performance with temperature for the Pt/C and PtRu/C catalysts, compared to Pt_3Sn/C, which monotonically increases with the temperature.

Significant information could be obtained from the estimation of the apparent activation energy as widely reported in the literature [21, 28, 36–38]. Figure 4 shows the Arrhenius' plots for the different catalysts. In order to minimize effects associated to limitations in the current density by ohmic and/or mass transfer polarizations, the currents were reported with respect to the open circuit voltage (OCV) considering an overvoltage of 50 mV (defining the actual voltage for this measurement as the subtraction of 50 mV from the OCV). Lower overvoltages were not considered due to possible crossover that also may mask actual results. It can be observed that, in the case of Pt/C, there exist two well defined regions, one between

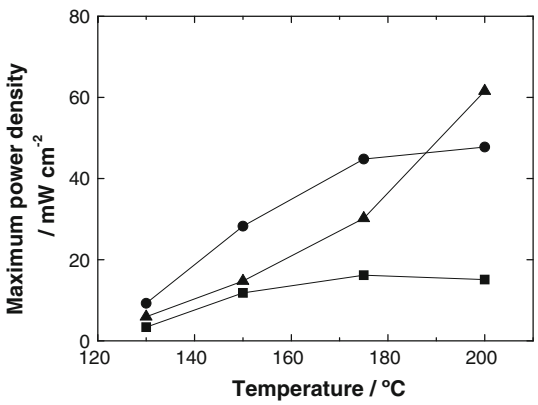

Fig. 3 Evolution of the maximum power density drawn from the cell with the temperature for the different catalysts (*filled square* Pt/C, *filled circle* PtRu/C, *filled triangle* Pt_3Sn/C)

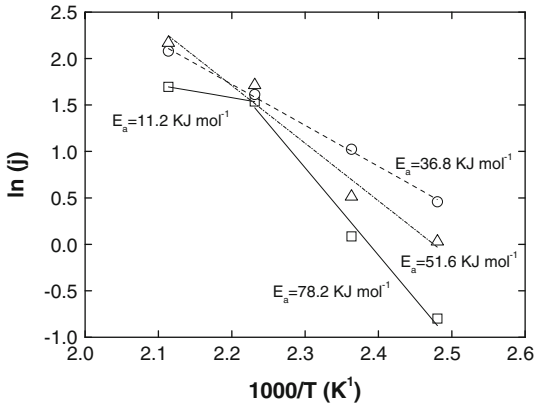

Fig. 4 Arrhenius plots for the different catalysts at an overpotential of 50 mV (*open square* Pt/C, *open circle* PtRu/C, *open triangle* Pt_3Sn/C)

130 and 175 °C, with an activation energy of 78.2 kJ mol^{-1}, and a second one where there is a significant drop in the activation energy, with a value of 11.3 kJ mol^{-1}. In the case of PtRu/C, the experimental data fit well to the Arrhenius law in the considered temperature range, indicative of a single oxidation mechanism. The corresponding value of the activation energy was 36.8 kJ mol^{-1}. In the case of the Pt_3Sn/C, although the data show Arrhenius behaviour, the quality is lower than in the case of PtRu/C, revealing that the mechanism could change as the temperature increases. Moreover, the reported value of the activation energy is higher and corresponds to 51.6 kJ mol^{-1}.

The ethanol electrooxidation mechanism can be derived from the product distribution. The considered ethanol oxidation residues obtained were acetaldehyde, acetic acid, ethyl acetate, carbon dioxide and methane. Traces of other products, such as ethane and ethylene were detected. However, the corresponding concentrations did not significantly alter the percentage of the just cited most significant species. On the other hand, ethyl acetate was transformed to acetic acid according to the following reaction (Eq. 1).

$$CH_3COOC_2H_5 + H_2O \rightarrow CH_3COOH + C_2H_5OH \quad (1)$$

Another important feature to be mentioned is the presence of some residues at OCV conditions. Two could be the ways for forming such products: (i) oxygen crossing from the cathode to the anode through the membrane, or (ii) non-electrochemical processes. Oxygen crossing is disregarded since measurements of the oxygen permeability of the H_3PO_4-doped m-PBI membranes showed negligible values. Therefore, the process (ii) is more likely to be responsible for the appearance of those products. Detected products at OCV were: acetaldehyde, acetic acid, ethyl acetate, methane and carbon dioxide. No hydrogen was detected. According to the literature, the reactions that may be occurring in the system are [28, 39, 40]:

$$CH_3CH_2OH \rightarrow CH_3CHO + 2H_{ads} \quad (2)$$

$$CH_3CHO + H_2O \rightarrow CH_3COOH + 2H_{ads} \quad (3)$$

$$CH_3CHO \rightarrow CO + CH_4 \quad (4)$$

$$CO + 6H_{ads} \rightarrow CH_4 + H_2O \quad (5)$$

$$CO + H_2O \rightarrow CO_2 + 2H_{ads} \quad (6)$$

Reaction (2) corresponds to the alcohol dehydrogenation, reported to happen on platinum at temperatures below 350 °C [39]. The acetaldehyde formed can be further oxidized with water to form acetic acid, or decomposed to carbon monoxide and methane according to reaction 4. The carbon monoxide produced can follow two pathways: (i) it can undergo a methanation process, producing more methane, or, it can be converted into carbon dioxide through the water gas shift reaction. The presence of the other species, ethylene and ethane can be explained in terms of the dehydration of ethanol to form ethylene, according to reaction 7:

$$CH_3CH_2OH \rightarrow CH_2 = CH_2 + H_2O \quad (7)$$

The formation of ethane is attributed to the hydrogenation of the ethylene generated during the dehydration of the ethanol molecule (reaction 8):

$$CH_2 = CH_2 + 2H_{ads} \rightarrow CH_3{-}CH_3 \quad (8)$$

The following procedure will be applied to interpret the product distribution. The number of moles of each product obtained after the polarization of the cell will be subtracted from the ones measured at OCV. One important issue to point out in this calculation is the appearance of methane generated "electrochemically". In order to understand this, it is necessary to adopt an ethanol electrooxidation model. One very useful option is the combination of the traditional ones [20, 32, 41], depicting the formation of acetaldehyde, acetic acid, ethyl acetate and carbon dioxide, combined with the one proposed by Otomo et al. [28]. Figure 5 shows a simplified scheme of the possible electrooxidation pathways. Hence, the electrochemical generation of methane comes accompanied with the generation of carbon dioxide, and, in this case, only four electrons are produced compared to the 12 coming from the complete oxidation.

Figure 6 displays the corresponding molar percentages for acetaldehyde in the different catalysts, temperatures and current densities. As it can be seen, acetaldehyde is, overall, the main oxidation product for the three catalysts. Nevertheless, Pt/C displays the lowest acetaldehyde percentages, indicating that this catalyst significantly favours further oxidative routes. In fact, Pt/C shows a decrease in the acetaldehyde percentage up to 175 °C, decreasing down to 45 % at 175 °C. Nonetheless, the operation at 200 °C boosts the production of acetaldehyde again in electrochemical terms. In the case of Pt_3Sn/C, the percentage of acetaldehyde constantly decreases with the increase of temperature and current density, suggesting that both conditions are more favourable for electrogeneration of more oxidized products. In the case of PtRu/C, overall, acetaldehyde is the main oxidation product, observing simply a tiny decrease in the percentage at higher current densities and temperatures. Values are always above 90 % of the total oxidation product.

Figure 7 shows the corresponding molar percentage for acetic acid. According to the results, acetic acid is not the main product of ethanol oxidation at high temperatures. Acetic acid is relatively significant for Pt/C and Pt_3Sn/C at high current densities and temperatures. In the case of the PtRu/C catalyst, although the percentage is too low

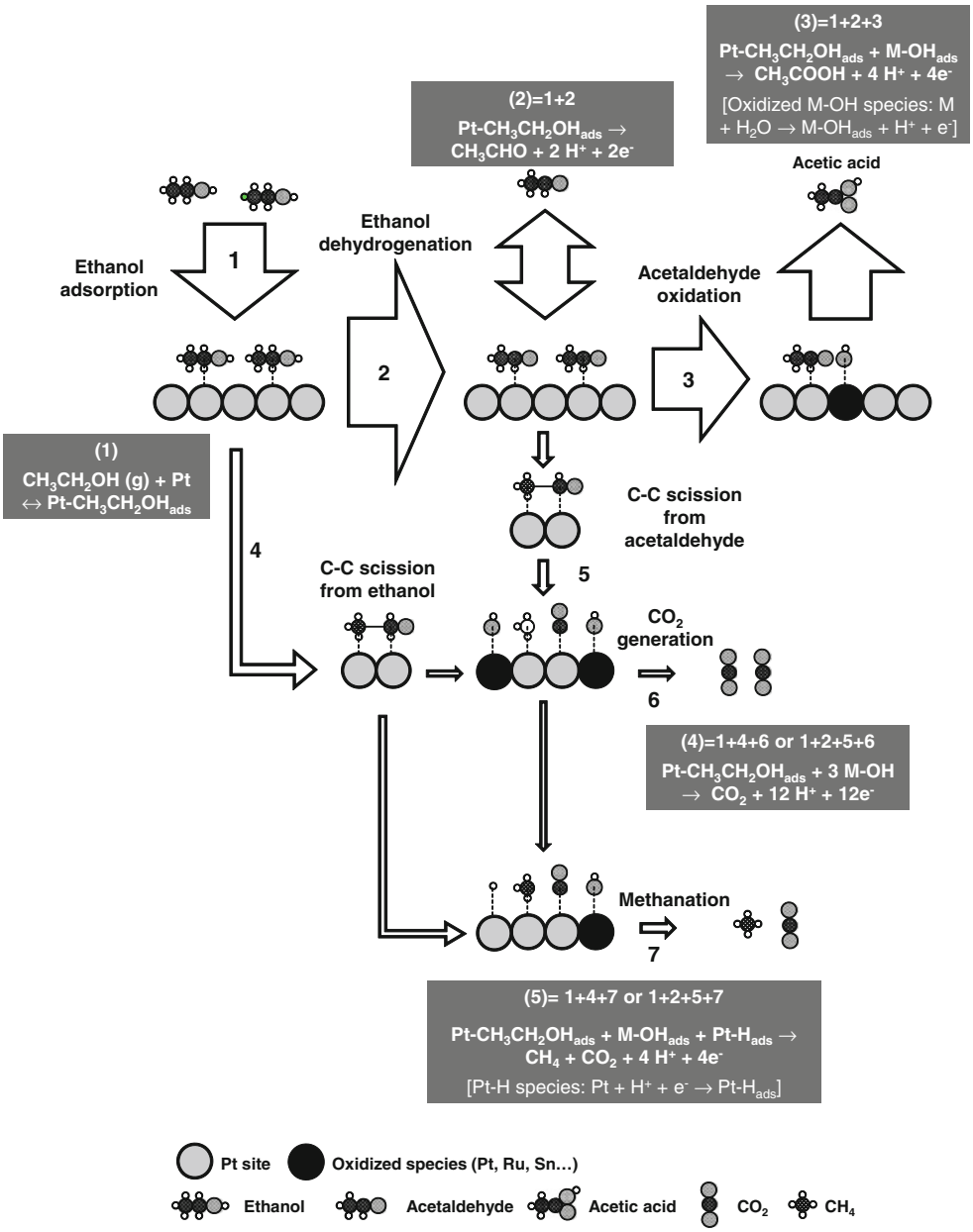

Fig. 5 Schematic diagram of the different ethanol electrooxidation routes

compared to the other catalysts, there is also an increase with the current density. However, the temperature does not exert the same effect, showing, in fact, a drop in the acid percentage.

Figure 8 displays the carbon dioxide percentages for the catalysts at the different temperatures and current densities. Pt/C is the catalyst showing the largest percentage of carbon dioxide, compared to Pt_3Sn/C, and particularly to PtRu/C, which produces a minimum amount of CO_2. Compensating the drop in the acetaldehyde percentage, the amount of carbon dioxide is maximum at 175 °C for Pt/C, attaining values as high as 56 %. However, at 200 °C, there is a notable decrease in the percentage, indicating that this electrochemical route is limited in favour of the C_2-route. In the case of Pt_3Sn/C, the proportion of CO_2 is lower compared to Pt/C, but contrarily to Pt/C, it follows the expected trend of increase in the CO_2 percentage with the temperature. Finally, in the case of the PtRu/C catalyst, the percentage is rather low, below 5 %, implying that this catalyst does not favour the scission of the C–C bond. Figure 8 also includes the CO_2 percentages corresponding to the incomplete oxidation accompanied with methane generation. This parameter is important since the CO_2 produced by this route, even with C–C scission, yields only four electrons compared to the 12 electrons per ethanol molecule linked to the complete oxidation. When the cell temperature was increased up to 200 °C, within the fact that electrochemical C_1-route is disfavoured in the cases of

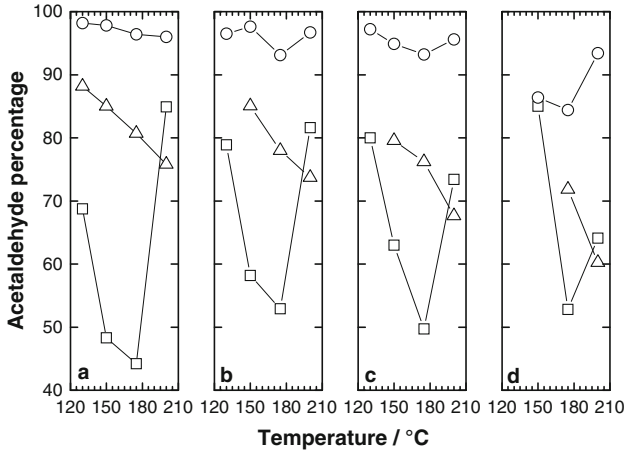

Fig. 6 Acetaldehyde percentage at different temperatures at **a** 20 mA cm^{-2}, **b** 40 mA cm^{-2}, **c** 60 mA cm^{-2}, **d** 100 mA cm^{-2} (*open square* Pt/C, *open circle* PtRu/C, *open triangle* Pt_3Sn/C)

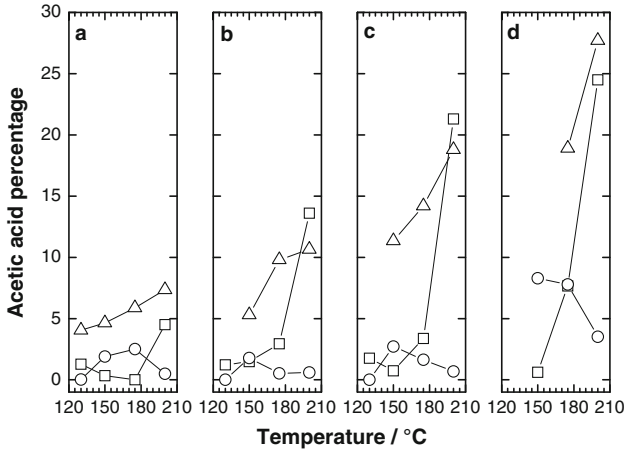

Fig. 7 Acetic acid percentage at different temperatures at **a** 20 mA cm^{-2}, **b** 40 mA cm^{-2}, **c** 60 mA cm^{-2}, **d** 100 mA cm^{-2} (*open square* Pt/C, *open circle* PtRu/C, *open triangle* Pt_3Sn/C)

Pt/C and PtRu/C, the incomplete C_1 electrochemical route leading to the electrogeneration of methane, becomes prominent compared to the complete oxidation, visible by the percentages of methane close to those of carbon dioxide at 200 °C.

Figure 9 shows the CH_4 molar percentages at the different temperatures and current densities for the Pt/C, PtRu/C and Pt_3Sn/C catalysts. Despite CH_4 is not actually an oxidized product from ethanol, the analysis is of interest, since it reveals the existence of an electroreduction process. Methane has been widely recognized as a by-product of the ethanol reforming process, from acetaldehyde decomposition (reaction 4) and formation of CH_4 (reaction 5), happening on metals such as platinum, iridium, cobalt, nickel and ruthenium [39, 40, 42–45]. Nevertheless, few studies [28, 46–48] reported its presence in the electrooxidation of

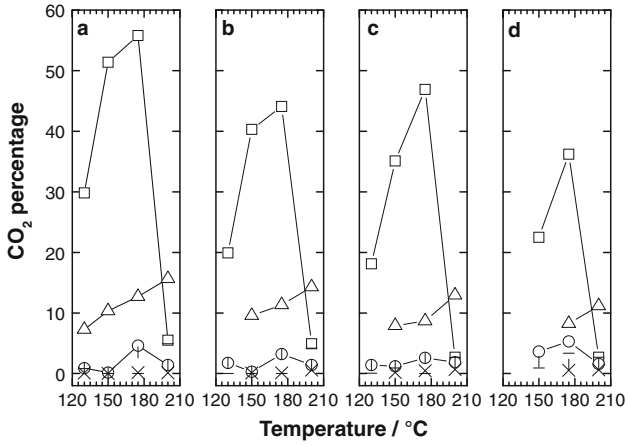

Fig. 8 Carbon dioxide percentage at different temperatures at **a** 20 mA cm^{-2}, **b** 40 mA cm^{-2}, **c** 60 mA cm^{-2}, **d** 100 mA cm^{-2} (overall CO_2 percentage: *open square* Pt/C, *open circle* PtRu/C, *open triangle* Pt_3Sn/C; CO_2 associated to the CH_4 electrogeneration: − Pt/C, *open square* PtRu/C, + Pt_3Sn/C)

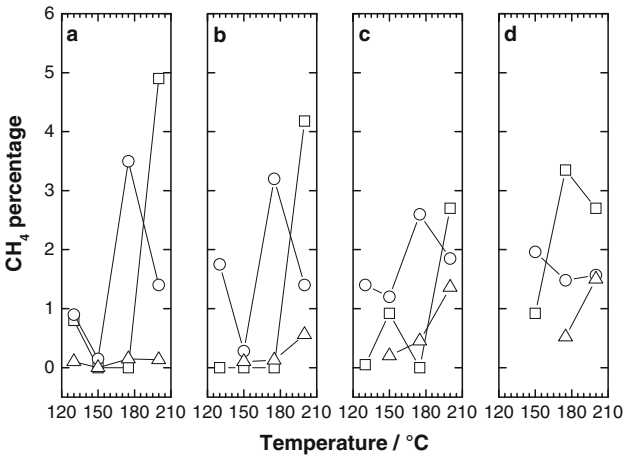

Fig. 9 Methane (electrochemically produced) percentage at different temperatures at **a** 20 mA cm^{-2}, **b** 40 mA cm^{-2}, **c** 60 mA cm^{-2}, **d** 100 mA cm^{-2} (*open square* Pt/C, *open circle* PtRu/C, *open triangle* Pt_3Sn/C)

ethanol on platinum, coming from the hydrogenation of the Pt–CH_x produced after the C–C scission. This study confirms its presence, which is deleterious from the point of view of efficiency, owing to the consumption of H_{ads} species, which could contribute for producing more electrons (route 5 in Fig. 5). This impacts on the assessment of the number of electrons used in the ethanol oxidation, as discussed below. Important facts are that only Pt/C and PtRu/C show some methane generation, contrarily to Pt_3Sn/C that hardly presents this phenomenon. It is also shown that the higher the temperature the larger the amount of methane produced. Finally, the operation at high current densities reduces the formation of methane.

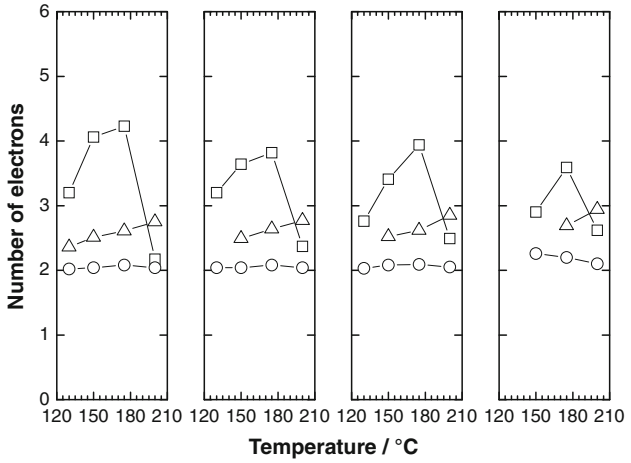

Fig. 10 Number of electrons used in the ethanol electrooxidation at different temperatures at 20 mA cm^{-2}, 40 mA cm^{-2}, 60 mA cm^{-2} and 100 mA cm^{-2}. Figures places consecutively (*open square* Pt/C, *open circle* PtRu/C, *open triangle* Pt_3Sn/C)

Figure 10 shows the number of electrons obtained after the ethanol oxidation considering the different electrochemical products as depicted in Fig. 5, calculated by applying Eq. 9 [49].

$$n = \frac{1}{\sum_i q_i/n_i} \text{ where } q_i = \frac{n_i f_i F}{\sum_i n_i f_i F} \quad (9)$$

The parameter f_i represents the mole fraction of each product, F is the value of the Faraday constant, and n_i is the number of electrons associated to the corresponding species.

As it can be seen, the most effective catalyst for ethanol oxidation is Pt/C up to 175 °C, producing between 3 and 4 electrons. At 200 °C, there is a dramatic decrease in the number of electrons to a value slightly above of 2, and consequently in the faradaic efficiency, revealing a less efficient oxidation. In the case of PtRu/C, there is almost no change in the amount of electrons, constrained in the range of 2–2.2 electrons. This reveals a low efficiency electrochemical oxidation in the whole range of conditions studied. Finally, Pt_3Sn/C shows a slow but constant increase in the number of electrons with the temperature, reflecting the beneficial effect of operating at higher temperatures with this catalyst. On the other hand, in terms of increasing current density, for the Pt/C catalyst there is a decrease in the number of electrons, whereas in the cases of PtRu/C and especially Pt_3Sn/C, the operation at high current densities promotes the generation of more electrons.

4 Discussion

From the X-ray diffractograms, the three commercial catalysts present crystal sizes in the nanometric range, small enough to guarantee satisfactory surface areas. Yet, the most interesting information comes from the lattice parameter, where there is a displacement from that corresponding to Pt/C. This indicates that these metals formed fcc alloys with platinum. In the case of ruthenium, the smaller atomic radius leads to a contraction of the lattice parameter, contrarily to Sn. Nevertheless, the degree of alloy of PtRu/C is lower than that of Pt_3Sn/C, where most of the tin is alloyed with Pt forming the intermetallic Pt_3Sn compound. This result is important since the formation of a Pt_xM_y alloy directly impacts on the mechanism for ethanol oxidation, and therefore, the cell performance. Spatial and electronic effects are responsible for such differences. In the formation of alloys, there is a more intimate contact between the atoms of the two metals, aside from stronger electronic effects that modify the 5d-band of platinum. XAS analyses carried out by this research group have demonstrated that: (a) formation of a PtRu solid solution leads to a weakening of the adsorption strength on the surface of platinum sites [50], (b) the presence of a Pt_3Sn phase reinforce the adsorption strength of adsorbates on the surface of the active platinum sites [51].

The polarization curves (Fig. 2) show a significant enhancement in the cell performance when bimetallic catalysts are used. As mentioned above, this well-known behaviour can be explained in terms of the bifunctional mechanism, assisting in the donation of –OH species from the second metal at lower potentials than platinum. A second promoting mechanism is the ligand effect. A change in the electronic environment of platinum can also promote the ethanol oxidation. This is especially significant in the formation of the Pt_3Sn intermetallic compound, as demonstrated by Xu and Wang [52] DFT studies, favouring the dehydrogenation step of the α- and the hydroxyl hydrogen. In the case of Pt_3Ru, the promotion is present to a lower extent. The combination of those two effects enhances the ethanol oxidation rate compared to Pt/C. In fact, this particular promotion mechanism of Pt_3Sn/C can explain the monotonous increase of the performance with the temperature, contrarily to Pt/C and PtRu/C. Furthermore, the crystalline Pt_3Sn phase reinforces the adsorption strength on the platinum surface, in a more favourable environment for further oxidation of the ethanol molecule, as shown by the results in Figs. 7 and 9 (larger percentages of acetic acid and CO_2), becoming the oxidation more efficient compared to PtRu/C. In the PtRu/C catalyst, the expected lower adsorption strength of ethanol on the platinum surface could only promote the dehydrogenation of ethanol to acetaldehyde, as the product distribution (Fig. 6) suggests. The fuel cell results (Figs. 2, 3) indicate, on the other hand, that this process happens at a high turnover rate. Pt/C displays, at 200 °C, no improvements in the performance. At this temperature, there is a drastic increase of the acetaldehyde

percentage, turning the ethanol electrooxidation less effective as in the case of PtRu/C, limiting the cell performance in terms of current density.

All the mentioned trends reflect on the different values of the activation energy of each catalyst. In the case of Pt/C, there is a change in the slope at 175 °C, indicating a change in the mechanism for ethanol electrooxidation. This actually reflects on the product distribution. Above that temperature, acetaldehyde becomes the most favoured electrooxidation product, and this oxidation route is known to possess a lower activation barrier than the one leading to CO_2 [21]. This result resembles that of Camargo et al. [53], who already observed a change in the activation energy for a Pt/C catalyst oxidizing ethanol at high temperature in concentrated H_3PO_4. They also suggested a change in the mechanism for ethanol oxidation as the origin for the reduction in the activation energy. PtRu/C fits to Arrhenius' law in the whole range of temperature, indicating that there are no changes in the mechanism with temperature. In fact, the almost single oxidation product in the whole range of operating conditions was acetaldehyde. Finally, the results on Pt_3Sn/C also follow Arrhenius' law, displaying a higher value of the activation energy. This, in agreement with the product distribution and the number of electrons linked to the ethanol electrooxidation, is ascribed to an oxidation route leading to more oxidized products.

Product distribution results show that the Pt/C catalyst produces the lowest acetaldehyde percentage and leads to the highest values for CO_2 linked to the complete conversion of ethanol. Pt/C has been reported as a very effective catalyst for ethanol oxidation, and indeed several studies show that this catalyst presents the highest percentages for complete ethanol conversion [30, 32, 33, 54, 55]. The increase in the temperature favours the complete conversion to CO_2, since more energy is available in the system for breaking the C–C bond. However, this route gets disfavoured when the current density increases. At high current densities, high turnover rates are required, and the complete oxidation of ethanol to CO_2 becomes limited as reported by Rao et al. [56]. That process requires longer adsorption times for breaking the C–C bond, promoting the generation of acetic acid from the oxidation of acetaldehyde by donation of Pt–OH species present on the platinum surface. Pt/C presents a detrimental drop in the percentage of CO_2 at 200 °C, accompanied with an increase in the generation of methane. Greater amounts of methane were detected at this temperature under OCV conditions compared to the others temperatures (more than 10 times, whereas between 130 and 175 °C remained almost constant). This ability of platinum for forming methane at intermediate temperatures in the range of 200–250 °C [39] leads to an intense "non-electrochemical" activity, which appears to limit the complete oxidation of the ethanol molecule to CO_2 in favour of the incomplete one. The more limited number of available neighbouring Pt active sites required for the electrochemical breakage the C–C bond could explain the promotion of the C_2 oxidation route. This directly impacts on the number of electrons, which drastically drops as shown in Fig. 10.

The PtRu/C catalyst is very effective in activating the oxidation reaction, increasing significantly the current density. However, ruthenium significantly depresses the capacity for complete oxidation of the ethanol molecule. Large percentages of acetaldehyde are observed on this catalyst for all the experimental conditions studied. Reasons for such a behaviour lie on the ligand effect that this metal presents on platinum, weakening the adsorbate strength on the platinum sites. Further, the presence of Ru ad-atoms on platinum turns more difficult the C–C cleavage, since, as above mentioned, several neighbouring platinum sites are needed for such a process. The combination of these two effects results in very low CO_2 percentages. In addition, low acetic acid percentages are displayed for this catalyst. The weaker adsorption of the CH_3CHO_{ads} can limit its further oxidation to CH_3COOH in spite of the presence of oxygenated species on the surface of the catalyst even at low potentials (Ru–OH). Finally, the low CO_2 percentages are linked to the inefficient generation of CH_4. Ruthenium is known as a good catalyst for processes that form methane, so its presence may promote this route, disfavouring the complete oxidation of the $Pt–CH_x$ species produced after the C–C scission [43]. The very low efficiency in ethanol oxidation explains the reduced number of electrons produced. Further, this number almost does not change over the whole operational conditions, corroborating that the ethanol electrooxidation mechanism does not change. This is consistent with the constancy of the activation energy measured.

The Pt_3Sn/C catalyst also leads to acetaldehyde as the main oxidation product, but to a lower extent compared to PtRu/C. More oxidized products, such as acetic acid at high current densities and CO_2 at high temperatures, are obtained. The ligand effect of Sn when alloyed with Pt, strengthening the ethanol adsorption, can be responsible for the larger percentages of CO_2, despite the presence of tin atoms on the surface of the catalyst may hinder the C–C cleavage. Further, although it may seem contradictory, the stronger adsorption might be responsible for the inferior performance compared to PtRu/C below 175 °C, due to a certain poisoning effect on the platinum sites by the electrogenerated adsorbates, in spite of the presence of –OH species at low potentials from the Sn atoms on the surface. The temperature, as in the case of Pt/C, exerts a beneficial effect by providing more energy for breaking the C–C bond. On the other hand, the presence of those more readily oxidizable Sn atoms on the surface leads to higher acetic

acid percentages compared to the other catalysts, turning the oxidation more effective compared to PtRu/C. This reflects on the higher number of electrons, and on the higher activation energy in Fig. 5, and indeed could explain the highest performance at 200 °C. One remarkable feature is that, contrarily to Pt/C and PtRu/C, the electrogeneration of CH_4 is minimal, and indeed, almost negligible amounts of methane were detected in the anode exhaust. This can be explained taking into account that tin is known as an anti-methanation catalyst in heterogeneous catalysis, favouring, for instance, water gas shift reactions instead of formation of methane in the presence of syngas (H_2 + CO) [57].

In summary, Pt/C emerges as the most effective catalyst for the electrooxidation of ethanol, achieving large percentages of complete conversion to CO_2. Nevertheless, it undergoes a detrimental formation of methane that decreases the number of electrons used when operating at temperatures above 200 °C. Its weakest feature is the poorer performance, in terms of current generation, compared to PtRu/C and Pt_3Sn/C due to a significant poisoning of the platinum sites by the ethanolic residues, only overtaken at high anode overpotentials. In the PtRu/C catalyst, the presence of Ru assists in increasing the activity for ethanol oxidation, reflected on an increase in the turnover rate of ethanol molecules being oxidized to acetaldehyde. However, this product was uniquely favoured compared to more oxidized ones, turning the oxidation inefficient. The Pt_3Sn/C catalyst also promotes the ethanol oxidation, primarily to acetaldehyde, and this further gets oxidized to acetic acid by the –OH species on the surface provided by the more readily oxidizable tin atoms. The stronger adsorption of the ethanol molecule on the platinum sites promotes the C–C cleavage, producing intermediate CO_2 percentages between the least efficient PtRu/C and the most efficient Pt/C. Furthermore, this catalyst does not favour the generation of methane at high temperatures. As a consequence, the combination of a satisfactory cell performance and conversion of ethanol to carbon dioxide could tentatively lead to conclude that Pt_3Sn/C might be an attractive catalyst for application in high temperature DEFC, although further studies, especially those related to long-term stability are paramount in order to confirm its suitability. It is important to note that these results were obtained under high ethanol concentrations. These do not favour the complete oxidation [21], due to the lower water activity from which oxygenated species will be obtained in order to oxidize the ethanol residues. However, those high concentrations are more attractive from a practical point of view, and also, in terms of an enhanced cell performance. Finally, more advanced designs need to be proposed in order to further increase the cell performance improving, or at least maintaining, the CO_2 percentages. An interesting alternative could be structures with strong electronic effects that reinforce the ethanol adsorption on the platinum sites (metals donating electronic density) combining with sources of oxygenated species on the surface that allow the oxidation at high turnover rates of the ethanolic residues (RuO_x or SnO_x), on a platinum-enriched surface. This might be the way to obtain mainly the completely oxidized C_1 product: CO_2. In this sense, advanced core–shell-like structures decorated with metal oxides could be of interest.

5 Conclusions

The use of commercial PtRu/C and Pt_3Sn/C catalysts in PBI-based high temperature DEFC results beneficial in terms of fuel cell performance, assessed by the maximum power density, compared to Pt/C. However, each catalyst displays a different route for the ethanol oxidation, which indeed can be responsible for the different results. Pt/C is the most effective catalyst in terms of complete oxidation of the ethanol molecule to CO_2, achieving percentages as high as 55 % even with an ethanol concentration of 6.7 M. However, it also produces a significant amount of methane that reduces the number of electrons used and the performance when operated at 200 °C. PtRu/C with a partial degree of alloy of Ru with Pt, displays a higher activity reflected by the larger current densities compared to Pt/C. However, the dehydrogenation of acetaldehyde is significantly favoured, in an inefficient ethanol oxidation. Finally, Pt_3Sn/C, with an almost complete degree of alloy of Sn with Pt, displays the best trade-off between performance and ability for oxidizing the ethanol molecule. It shows an enhanced performance compared to Pt/C, and more oxidized products are obtained from the ethanol oxidation, achieving CO_2 percentages of almost 20 % when operated at 200 °C. In addition, it hardly presents the detrimental effect of methane formation. Tentatively, alloyed PtSn/C-based catalysts can be proposed as interesting candidates for high temperature PEM-based DEFC: enhanced performance, no formation of methane at high temperatures and capacity for further oxidation of the ethanol molecule compared to PtRu/C. This comes from tuning an adequate electronic effect with the bifunctional assistance. Nonetheless, further improvements in catalyst formulation are undoubtedly required.

Acknowledgments Authors want to thank to the Fundação de Amparo à Pesquisa do Estado de São Paulo (FAPESP), the Conselho Nacional de Desenvolvimento Científico e Tecnológico (CNPq), and the Coordenação de Aperfeiçoamento de Pessoal de Nível Superior (CAPES) for the financial support. In particular, Thairo A. Rocha thanks to the CNPq (Proc. 160459/2011-7) for a Master Degree scholarship, Sabrina C. Zignani thanks CNPq (Proc. 141545/2009-7)

for a doctoral scholarship, and José J. Linares thanks FAPESP for a post-doctoral fellowship (Proc. 2010/07108-3).

References

1. Lamy C, Countanceau C, Leger J-M (2009) The direct ethanol fuel cell: a challenge to convert bioethanol cleanly into electric energy. In: Barbaro P, Bianchini C (eds) Catalysis for sustainable energy production, 1st edn. Wiley, Weinheim, p 22
2. Snyder K (2009) New catalyst paves the path for ethanol-powered fuel cells. Brookhaven National Laboratory News. http://www.bnl.gov/bnlweb/pubaf/pr/PR_display.asp?prID=898. Accessed 25 July 2012
3. Wang J, Wasmus S, Savinell RF (1995) Evaluation of ethanol, 1-propanol, and 2-propanol in a direct oxidation polymer-electrolyte fuel cell. A real-time mass spectrometry study. J Electrochem Soc 142:4218–4224
4. Wainright JS, Wang J-T, Weng D, Savinell RF, Litt M (1995) Acid-doped polybenzimidazoles: a new polymer electrolyte. J Electrochem Soc 142:L121–L123
5. Lobato J, Cañizares P, Rodrigo MA, Linares JJ, Manjavacas G (2006) Synthesis and characterisation of poly[2,2-(*m*-phenylene)-5,5-bibenzimidazole] as polymer electrolyte membrane for high temperature PEMFCs. J Membr Sci 280:351–362
6. Linares JJ, Sanches C, Paganin VA, Gonzalez ER (2012) Poly(2,5-bibenzimidazole) membranes: physico-chemical characterization focused on fuel cell applications fuel cells, electrolyzers, and energy conversion. J Electrochem Soc 159(7):F194–F202
7. Qingfeng L, Hjuler HA, Bjerrum NJ (2001) Phosphoric acid doped polybenzimidazole membranes: physiochemical characterization and fuel cell applications. J Appl Electrochem 31: 773–779
8. Lobato J, Cañizares P, Rodrigo MA, Linares JJ (2009) Testing a vapour-fed PBI-based direct ethanol fuel cell. Fuel Cells 9: 597–604
9. Zhou Q, Zhou Z, Song S, Li W, Sun G, Tsiakaras P, Xin Q (2003) Pt based anode catalysts for direct ethanol fuel cells. Appl Catal B Environ 46:273–285
10. Tsiakaras PE (2007) PtM/C (M = Sn, Ru, Pd, W) based anode direct ethanol-PEMFCs: structural characteristics and cell performance. J Power Sources 171:107–112
11. Linares JJ, Rocha TA, Zignani S, Paganin VA, Gonzalez ER (2012) Different anode catalyst for high temperature polybenzimidazole-based direct ethanol fuel cells. Int J Hydrogen Energ. doi:10.1016/j.ijhydene.2012.06.113
12. Zhou WJ, Li WZ, Song SQ, Zhou ZH, Jiang LH, Sun GQ, Xin Q, Poulianitis K, Kountou S, Tsiakaras P (2004) Bi- and tri-metallic Pt-based anode catalysts for direct ethanol fuel cells. J Power Sources 131:217–223
13. Tayal J, Rawat B, Basu S (2012) Effect of addition of rhenium to Pt-based anode catalysts in electro-oxidation of ethanol in direct ethanol PEM fuel cell. Int J Hydrogen Energ 37:4597–46050
14. Ribeiro J, Dos Anjos DM, Léger J-M, Hahn F, Olivi P, De Andrade AR, Tremiliosi-Filho G, Kokoh KB (2008) Effect of W on PtSn/C catalysts for ethanol electrooxidation. J Appl Electrochem 38:653–662
15. Song S, He C, Liu J, Wang Y, Brouzgou A, Tsiakaras P (2012) Two-step sequence for synthesis of efficient PtSn@Rh/C catalyst for oxidizing ethanol and intermediate products. Appl Catal B Environ 30:227–233
16. Tripković AV, Lović JD, Popović KDJ (2010) Comparative study of ethanol oxidation at Pt-based nanoalloys and UPD-modified Pt nanoparticles. J Serb Chem Soc 75:1559–1574
17. Antolini E, Colmati F, Gonzalez ER (2007) Effect of Ru addition on the structural characteristics and the electrochemical activity for ethanol oxidation of carbon supported Pt–Sn alloy catalysts. Electrochem Comm 9:398–404
18. Antolini E (2007) Catalysts for direct ethanol fuel cells. J Power Sources 170:1–12
19. Parreira LS, Rascio DC, Silva JCM, De Souza RFB, D'Villa-Silva M, Calegaro ML, Spinacé EV, Neto AO, Santos MC (2012) A Pt_3Sn/C electrocatalyst used as the cathode and anode in a single direct ethanol fuel cell. Int J Chem 4:38–48
20. Léger J-M, Rousseau S, Coutanceau C, Hahn F, Lamy C (2005) How bimetallic electrocatalysts does work for reactions involved in fuel cells? Example of ethanol oxidation and comparison to methanol. Electrochim Acta 50:5118–5125
21. Sun S, Chojak Halseid M, Heinen M, Jusys Z, Behm RJ (2009) Ethanol electrooxidation on a carbon-supported Pt catalyst at elevated temperature and pressure: a high-temperature/high-pressure DEMS study. J Power Sources 190:2–13
22. Lobato J, Cañizares P, Rodrigo MA, Linares JJ (2009) Study of different bimetallic anodic catalysts supported on carbon for a high temperature polybenzimidazole-based direct ethanol fuel cell. Appl Catal B Environ 91:269–274
23. Lobato J, Cañizares P, Ubeda D, Pinar FJ, Rodrigo MA (2011) Testing PtRu/CNF catalysts for a high temperature polybenzimidazole-based direct ethanol fuel cell. Effect of metal content. Appl Catal B Environ 106:174–180
24. Parrondo J, Santhanam R, Mijangos F, Rambabu B (2010) Electrocatalytic performance of In_2O_3-supported Pt/C nanoparticles for ethanol electro-oxidation in direct ethanol fuel cells. Int J Electrochem Sci 5:1342–1354
25. Uda T, Boysen DA, Chisholm CRI, Haile SM (2006) Alcohol fuel cells at optimal temperatures batteries, fuel cells, and energy conversion. Electrochem Solid State Lett 9:A261–A264
26. Otomo J, Nishida S, Takahashi H, Nagamoto H (2008) Electro-oxidation of methanol and ethanol on carbon-supported Pt catalyst at intermediate temperature. J Electroanal Chem 615:84–90
27. Otomo J, Nishida S, Kato H, Nagamoto H, Oshima Y (2008) Direct alcohol electro-oxidation in an intermediate temperature fuel cell. ECS Trans 16:1275–1284
28. Shimada I, Oshima Y, Otomo J (2011) Acceleration of ethanol electro-oxidation on a carbon-supported platinum catalyst at intermediate temperatures. J Electrochem Soc 158:B368–B375
29. Zignani SC, Baglio V, Linares JJ, Monforte G, Gonzalez ER, Aricò AS (2012) Performance and selectivity of PtxSn/C electrocatalysts for ethanol oxidation prepared by reduction with different formic acid concentrations. Electrochim Acta 70:255–265
30. Nakagawa N, Kaneda Y, Wagatsuma M, Tsujiguchi T (2012) Product distribution and the reaction kinetics at the anode of direct ethanol fuel cell with Pt/C, PtRu/C and PtRuRh/C. J Power Sources 199:103–109
31. Wang Q, Sun GQ, Cao L, Jiang LH, Wang GX, Wang SL, Yang SH, Xin Q (2008) High performance direct ethanol fuel cell with double-layered anode catalyst layer. J Power Sources 177: 142–147
32. Rousseau S, Coutanceau C, Lamy C, Léger J-M (2006) Direct ethanol fuel cell (DEFC): electrical performances and reaction products distribution under operating conditions with different platinum-based anodes. J Power Sources 158:18–24
33. Andreadis G, Stergiopoulos V, Song S, Tsiakaras P (2010) Direct ethanol fuel cells: the effect of the cell discharge current on the products distribution. Appl Catal B Environ 100:157–164
34. Antolini E, Gonzalez ER (2011) Effect of synthesis method and structural characteristics of Pt–Sn fuel cell catalysts on the electro-oxidation of CH_3OH and CH_3CH_2OH in acid medium. Catal Today 160:28–38

35. Zhu M, Sun G, Xin Q (2009) Effect of alloying degree in PtSn catalyst on the catalytic behavior for ethanol electro-oxidation. Electrochim Acta 54:1511–1518
36. Colmati F, Antolini E, Gonzalez ER (2006) Effect of temperature on the mechanism of ethanol oxidation on carbon supported Pt, PtRu and Pt_3Sn electrocatalysts. J Power Sources 157:98–103
37. Sun S, Heinen M, Jusys Z, Behm RJ (2012) Electrooxidation of acetaldehyde on a carbon supported Pt catalyst at elevated temperature/pressure: an on-line differential electrochemical mass spectrometry study. J Power Sources 204:1–13
38. Jiang L, Colmenares L, Jusys Z, Sun GQ, Behm RJ (2007) Ethanol electrooxidation on novel carbon supported $Pt/SnO_x/C$ catalysts with varied Pt:Sn ratio. Electrochim Acta 53:377–389
39. Chiou JYZ, Siang J-Y, Yang S-Y, Ho K-F, Lee C-L (2012) Pathways of ethanol steam reforming over ceria-supported catalysts. Int J Hydrogen Energ. doi:10.1016/j.ijhydene.2012.02.081
40. Panagiotopoulou P, Verykios XE (2012) Mechanistic aspects of the low temperature steam reforming of ethanol over supported Pt catalysts. Int J Hydrogen Energ. doi:10.1016/j.ijhydene.2012.02.087
41. Lamy C, Lima X, LeRhun V, Delime F, Coutanceau C, Léger J-M (2002) Recent advances in the development of direct alcohol fuel cells (DAFC). J Power Sources 105:283–296
42. Zhao A, Ying W, Zhang H, Ma H, Fang D (2012) $Ni–Al_2O_3$ catalysts prepared by solution combustion method for syngas methanation. Catal Comm 17:34–38
43. Galleti C, Specchia S, Saracco G, Specchia V (2010) CO-selective methanation over $Ru–\gamma Al_2O_3$ catalysts in H_2-rich gas for PEM FC applications. Chem Eng Sci 65:590–596
44. Bao CL, Tsong TT (1988) Methanation on Ir surfaces at low gas pressure and temperature: a study by pulsed-laser field desorption time-of-flight mass spectroscopy. Surf Sci 201:371–384
45. Powell JB, Langer SH (1985) Low-temperature methanation and Fischer–Tropsch activity over supported ruthenium, nickel, and cobalt catalysts. J Catal 94:566–569
46. Kutz RB, Braunschweig B, Mukherjee P, Behrens RL, Dlott DD, Wieckowski A (2011) Reaction pathways of ethanol electrooxidation on polycrystalline platinum catalysts in acidic electrolytes. J Catal 278:181–188
47. Bittins-Cattaneo B, Wilhelm S, Cattaneo E, Buschmann HW, Vielstich W (1988) Intermediates and products of ethanol oxidation on platinum in acid solution. Phys Chem Chem Phys 92:1210–1218
48. Iwasita T, Pastor E (1994) A dems and FTir spectroscopic investigation of adsorbed ethanol on polycrystalline platinum. Electrochim Acta 39:531–537
49. Wang H, Jusys Z, Behm RJ (2004) Ethanol electrooxidation on a carbon-supported Pt catalyst: reaction kinetics and product yields. J Phys Chem B 108:19413–19424
50. Lima FHB, Gonzalez ER (2008) Ethanol electro-oxidation on carbon-supported Pt–Ru, Pt–Rh and Pt–Ru–Rh nanoparticles. Electrochim Acta 53:2963–2971
51. Colmati F, Gonzalez E (2007) Electronic effects in Pt-Sn alloy as anode in direct ethanol fuel cell. ECS Trans 11:1425–1435
52. Xu Z-F, Wang Y (2011) Effects of alloyed metal on the catalysis activity of Pt for ethanol partial oxidation: adsorption and dehydrogenation on Pt_3M (M = Pt, Ru, Sn, Re, Rh, and Pd). J Phys Chem C 115:20565–20571
53. Camargo APM, Previdello BAF, Varela H, Gonzalez ER (2010) Effect of temperature on the electro-oxidation of ethanol on platinum. Quim Nova 33:2143–2147
54. Ghumman A, Vink C, Yepez O, Pickup PG (2008) Continuous monitoring of CO_2 yields from electrochemical oxidation of ethanol: catalyst, current density and temperature effects. J Power Sources 177:71–76
55. Vigier F, Rousseau S, Coutanceau C, Leger J-M, Lamy (2006) Electrocatalysis for the direct alcohol fuel cell. Top Catal 40:111–121
56. Rao V, Cremers C, Stimming U, Cao L, Sun S, Yan S, Sun G, Xin Q (2007) Electro-oxidation of ethanol at gas diffusion electrodes A DEMS study. J Electrochem Soc 154:B1138–B1147
57. Polychronopoulou K, Kalamaras CM, Efstathiou AM (2011) Ceria-based materials for hydrogen production via hydrocarbon steam reforming and water-gas shift reactions. Recent Pat Mat Sci 4:1–24